

Comparison of ground-based and airborne transient electromagnetic methods for mapping glacial and permafrost environments: Cases from McMurdo Dry Valleys, Antarctica

Line M. Madsen^{a,*}, Thue Bording^{b,1}, Denys Grombacher^a, Nikolaj Foged^a, Neil Foley^c, Hilary A. Dugan^d, Peter T. Doran^e, Jill Mikucki^f, Slawek Tulaczyk^c, Esben Auken^a

^a HydroGeophysics Group, Department of Geoscience, Aarhus University, Aarhus, Denmark

^b Aarhus GeoInstrument, Aarhus, Denmark

^c Department of Earth and Planetary Sciences, University of California – Santa Cruz, Santa Cruz, CA, USA

^d Center for Limnology, University of Wisconsin – Madison, Madison, WI, USA

^e Department of Geology and Geophysics, Louisiana State University, Baton Rouge, LA, USA

^f Department of Microbiology, University of Tennessee, Knoxville, TN, USA

ARTICLE INFO

Keywords:

Electromagnetic theory
Antarctica
Hydrogeophysics
Transient EM

ABSTRACT

The transient electromagnetic (TEM) method is a non-invasive geophysical tool well-suited for subsurface imaging in cold and polar regions, where common targets are associated with strong contrasts in electrical resistivity. By imaging the electrical properties of the subsurface, the TEM methods can discriminate between geological units such as frozen ground (permafrost), fresh/saline groundwater systems, and bedrock/glacier ice. In this study, we compare TEM data acquired with ground-based and airborne TEM systems. We demonstrate the mapping capabilities of these two approaches in high latitude polar environments with datasets from Taylor Glacier, Lake Vanda, and Canada Glacier in the McMurdo Dry Valleys of Antarctica. The results show a high consistency between the airborne and ground-based TEM data, both with a high resolution and a deep penetration depth down to hundreds of meters due to the resistive background material, which makes both approaches capable of mapping hydrological systems and identifying the base of glaciers. The airborne TEM approach offers an unmatched spatial data coverage in difficult terrain and a far improved lateral resolution compared to the static ground-based system. The ground-based TEM system offers the possibility for using larger transmitter coils and longer stacking times and therefore has potential for reaching deeper penetration depths. The ground-based TEM approach is hence a valuable tool that can provide consistent imaging results while also being far more accessible in terms of cost and field logistics compared to an airborne TEM campaign.

1. Introduction

The conditions at the base of glaciers play important controls on glacial dynamics as they influence ice-flux rates, erosion rates of the underlying materials, and a number of other factors (e.g. Clarke, 2005; Smith et al., 2013). Direct sampling of subglacial conditions is often extremely challenging or infeasible due to difficult/unsafe terrain or significant ice thicknesses. In these cases, non-invasive imaging methods capable of mapping ice-thickness and the conditions at the base are

needed.

Ground-penetrating radar (GPR) is a common method for imaging glaciers, ice, and permafrost (e.g. Navarro and Eisen, 2009; Arcone and Kreutz, 2009; Shean and Marchant, 2010; Campbell et al., 2018). GPR is a high frequency (MHz to GHz range) electromagnetic method sensitive to contrasts in dielectric permittivity and electrical conductivity. The method thus provides high resolution of the depth to layer boundaries described by permittivity differences. The method is particularly well-suited to image glaciers and permafrost because ice and frozen ground

* Corresponding author at: Høegh-Guldbergsgade 2, DK-8000 Aarhus, Denmark.

E-mail addresses: linemeldgaard@geo.au.dk (L.M. Madsen), thue@aarhusgeoinstruments.dk (T. Bording), denys.grombacher@geo.au.dk (D. Grombacher), nikolaj.foged@geo.au.dk (N. Foged), hdugan@wisc.edu (H.A. Dugan), pdoran@lsu.edu (P.T. Doran), jmikucki@utk.edu (J. Mikucki), stulaczyk@ucsc.edu (S. Tulaczyk), ea@geus.dk (E. Auken).

¹ Formerly at Aarhus University.

typically have a high electrical resistivity (the reciprocal of the electric conductivity), meaning they are poor electrical conductors. The high resistivity ensures a low attenuation of electromagnetic energy so the radar waves can penetrate these materials down to hundreds of meters and can resolve both their total thickness and internal structures. However, the penetration depth becomes very shallow if electrically conductive materials such as brines, sediments, or soils of moderate electrical resistivity are present.

Time-domain (TEM) and frequency-domain (FEM) electromagnetics are another type of non-invasive imaging methods. These inductive EM methods can be deployed using both ground-based and airborne system configurations (e.g. Auken et al., 2017). Compared to GPR, FEM works in a lower frequency range (Hz-kHz), which in the time-domain corresponds to the ms-s time range. The EM methods image the electrical conductivity of the subsurface, where electrical conductivity contrasts are used to identify different subsurface units. For example, the resistivity ranges for glacier ice, permafrost, and unfrozen ground are well known and distinct; and these units can therefore often be distinguished by their resistivity values (Foley et al., 2016). Similar to GPR, EM also benefits from the absence of conductive units in resistive ice and permafrost environment, which leads to low attenuation of the EM signal and results in large penetration depths (>1000 m), which is much greater than that commonly imaged by EM in geological settings elsewhere (Spies, 1989). Even though EM is able to image layer boundaries, as a diffusive method it provides a poorer vertical resolution compared to GPR. However, EM has better ability than GPR to penetrate through electrically conductive materials (e.g. brines) – a consequence of the fact that the EM wave attenuation is frequency dependent and inductive EM methods work at lower frequencies than GPR does.

EM methods have previously been employed in polar settings, for instance for airborne surveys in Antarctica that aimed to map regional groundwater systems (Mikucki et al., 2015; Dugan et al., 2015), for ground-based and airborne measurements of sea ice thickness (Haas et al., 1997; Pfaffling et al., 2007), for measurements of extent of permafrost in Alaska (Minsley et al., 2012; Kass et al., 2021), and for identifying water-bearing unfrozen rock in Siberian permafrost (Kozhevnikov et al., 2014).

In this study, we focus on the TEM method. For surveys focusing on large and dense spatial coverage, the airborne TEM approach is the optimal choice compared to the ground-based approach, however, as we

will point out in the following, the ground-based approach is still valuable. Our goal in this paper is to validate and highlight the benefits of the ground-based TEM approach in polar settings through comparison with airborne TEM data collected over glaciers, permafrost, and frozen lakes in the McMurdo Dry Valleys in Antarctica. We present comparisons of ground-based and airborne sensitivity distributions and resistivity profiles to highlight consistency between the approaches, as well as to demonstrate their advantages. The chief advantages being the potential for larger penetration depths for ground-based systems, which is a consequence of the ability to use much larger transmitter coils and longer stacking times in a stationary system compared to the mobile requirements of an airborne setup, and the significantly reduced deployment costs (as no helicopter is required).

2. Data collection

Airborne and ground-based TEM data were collected in the McMurdo Dry Valleys in Antarctica in 2011 and 2018 (Fig. 1). The McMurdo Dry Valleys are hyper-arid polar deserts and represent a significant portion of the ice-free regions in Antarctica (e.g. Doran et al., 2002; Marchant and Head III, 2007; Kavanaugh and Cuffey, 2009; Levy, 2013).

In order to further the understanding of the hydrological systems in the McMurdo Dry Valleys, a proof-of-concept airborne TEM survey using a SkyTEM system (Sørensen and Auken, 2004b, specifications described later) was carried out in 2011 (Mikucki et al., 2015; Dugan et al., 2015; Foley et al., 2016). The survey detected low resistivity zones (10–800 Ωm) beneath the high resistivity glaciers and dry permafrost (500–20,000 Ωm and up to 500 m in thickness). The low resistivity zones were interpreted as partially frozen brine-bearing layers, where the high solute content of the pore water prevents freezing.

In 2017, a ground-based TEM survey was carried out using a ground-based TEM system developed in-house at the HydroGeophysics Group at Aarhus University (technical details described later). The ground-based survey had multiple purposes: to validate the use of the ground-based TEM method in polar environments; to validate the airborne data from 2011; to scout for new airborne targets and to target deeper structures. A total of 68 ground-based soundings were measured in the McMurdo Dry Valleys. Following the ground-based survey, another airborne survey with approximately 3500 line kilometers was carried out in 2018 to further study the subsurface water systems and surface

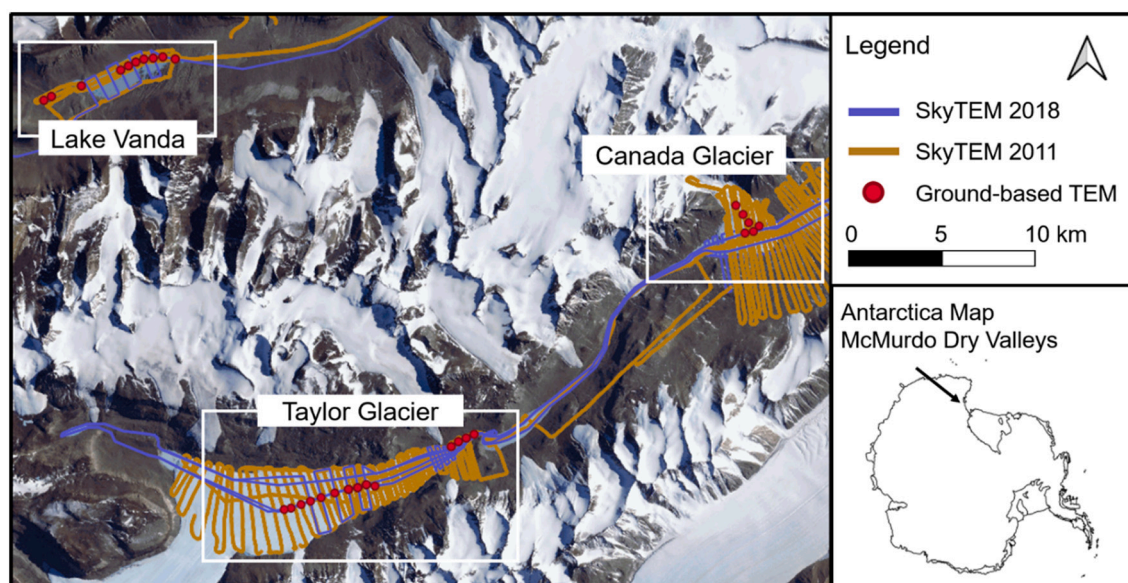


Fig. 1. Map of the area around Lake Vanda, Taylor Glacier, and Canada Glacier in the McMurdo Dry Valleys, Antarctica. Collected airborne SkyTEM data (orange and purple lines) and ground-based data (red circles) are overlain on survey targets. (For interpretation of the references to colour in this figure legend, the reader is referred to the web version of this article.)

hydrological connections (Foley et al., 2019) as well as geothermal heat-flux rates (Foley et al., 2020) on both new and previously studied areas.

In the following, we compare the 2011, 2018 airborne data and the 2017 ground-based data with a focus on the areas around Lake Vanda, Taylor Glacier, and Canada Glacier (Fig. 1).

3. The transient electromagnetic method

Transient electromagnetic measurement involves the use of a transmitter and a receiver coil. The measurement begins by building a strong steady current in the transmitter coil and thus a static primary magnetic field. Once the static field is established, the current is rapidly turned off. Turning off the current causes a flux change inducing eddy current in the ground. These eddy currents expand down and outwards away from the transmitter coil with time. As the currents decrease in magnitude and get dissipated into heat they induce themselves a time varying magnetic field, which can be measured as a voltage in a receiver coil. The magnitude and rate of decay is dependent on the conductivity of the subsurface layers in such a way that conductive layers causes slowly decaying fields while resistive layers causes fast decaying fields. One time-dependent voltage measurement is called a transient. Fig. 2a-2b illustrate the ground-based system used in this study with a 100×100 m transmitter loop and a 10×10 m receiver coil and Fig. 2c shows the applied airborne system.

The depth to which the subsurface can be reliably imaged by the TEM method is referred to as the depth of investigation (DOI) (Christiansen and Auken, 2012). Several factors influence the DOI such as the electrical resistivity structure of the subsurface, the transmitter magnetic moment (product of the effective coil area and the current strength), the noise level, and the data stack size (Spies, 1988; Spies, 1989). The DOI is deeper in a resistive setting compared to a conductive one. This means that the DOI for measurements conducted on a glacier (which has very high electrical resistivity) will be much larger than over seawater (which has very low electrical resistivity). This suggests that TEM is well-suited for identifying resistivity contrasts in polar/glacial settings where high resistive top layers (ice/permafrost/bedrock) are common and a high DOI can be expected.

One of the factors that can be manipulated in a TEM system in order to vary the strength of the TEM signal and thus influence the DOI, is the transmitter moment and thus influence the DOI, is the transmitter moment and the number of transients stacked. As such, increasing the stack size or increasing transmitter coil dimensions and increasing the transmitted currents, which increases the moment,

produce a deeper DOI.

In this study, so-called dual-moment TEM systems have been applied. In dual-moment systems, a low and a high amplitude current pulse are used in alternation to increase the resolution capabilities for both shallow and deep structures, (e.g. Sørensen and Auken, 2004). In practice, a number of low power current pulses is transmitted followed by a number of high power current pulses. Often, both the shape of the current waveform and the current amplitude are different for the low and high power pulses. At each point of measurement, the data is then measured as the response of first the low moment (LM) and then the high moment (HM), which produces two data curves for each measurement point. Fig. 3 shows examples of a ground-based and an airborne TEM

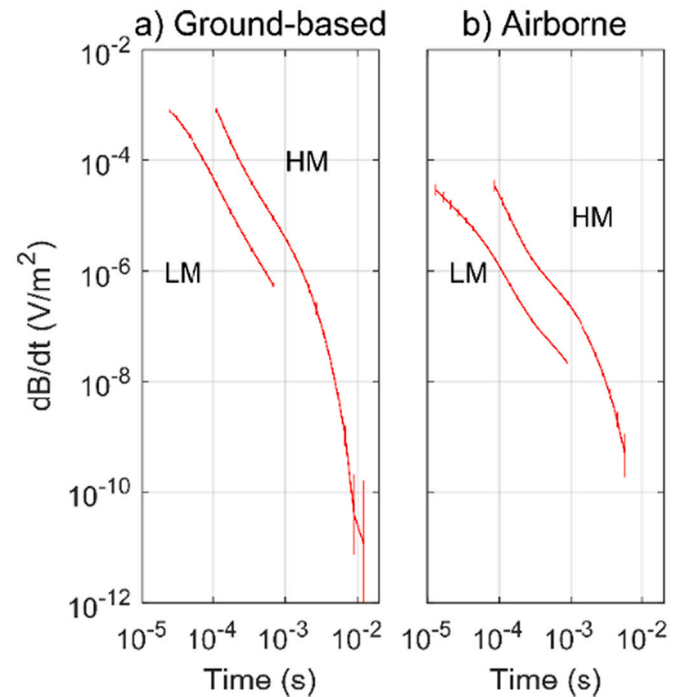


Fig. 3. Data example from Lake Vanda showing the low-moment (LM) and high-moment (HM) transients measured with the ground-based (a) and airborne TEM approach (b).

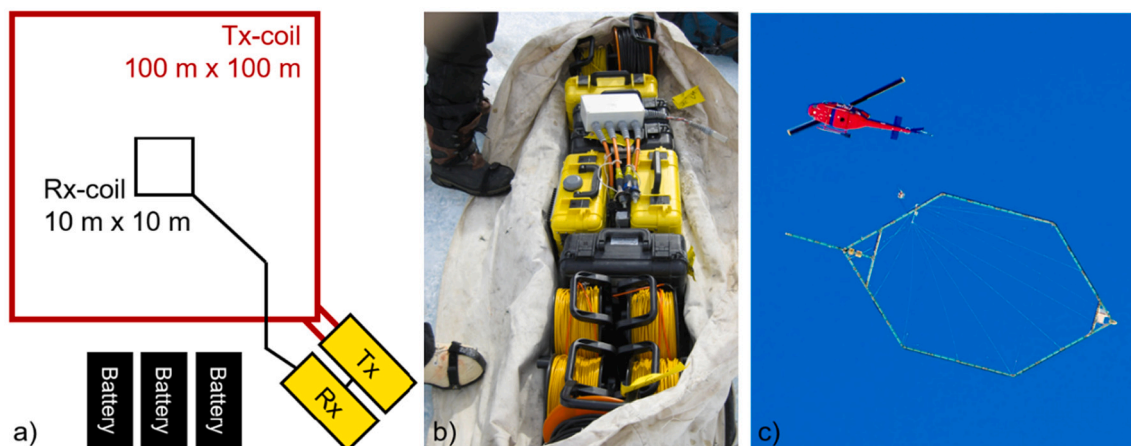


Fig. 2. a) Sketch of the ground-based TEM system setup with a 100×100 m transmitter (Tx) coil and 10×10 m two turn receiver (Rx) coil in a central-loop configuration. b) The ground-based TEM system packed on a sled. The yellow boxes contain the transmitter and receiver hardware and the black boxes are the batteries. The total load of the system applied was approximately 100 kg. c) The airborne TEM system with a 341 m^2 transmitter loop carried below a helicopter with the receiver coil placed just above the transmitter in the back of the loop. (For interpretation of the references to colour in this figure legend, the reader is referred to the web version of this article.)

data measurement from Lake Vanda. For both the LM and HM data, the measured time derivative of the magnetic field (dB/dt) is plotted as a function of time after the current is starting to shut down in the transmitter coil. Due to the differences in the LM and HM current waveform, the data are measured in different time gates (Fig. 3). The short LM waveform allows data collection at earlier times compared to HM. The high current amplitude used in the HM measurement increases the signal level and thus the signal-to-noise ratio, which allows data collection at later times where the signal level otherwise would be below the noise floor. Combined, this enhances the differences between the resolution capabilities of the LM and HM measurements, letting the LM resolve shallow structures and the HM the deeper ones (and thus controlling the DOI).

3.1. Airborne TEM

Airborne TEM systems use a transmitter coil that is either fixed to a rigid frame suspended beneath a helicopter or strung around the exterior of a fixed-wing aircraft (e.g. Sørensen and Auken, 2004; Witherly et al., 2004). For helicopter TEM, the receiver coil is placed in the center of the transmitter coil (a central-loop configuration) or in a zero-coupling position (with respect to the primary field) as shown in Fig. 2c. For fixed-wing TEM systems, the receiver coil is normally towed behind the aircraft in a small bird (an offset configuration). The dimension of the transmitter coil is limited by what can be picked up and stably flown by the aircraft. To increase the transmitter moment, the number of turns in the coil and the transmitted currents must therefore be increased instead of increasing the area.

In this study, two different SkyTEM systems have been used for data collection. In 2011, a SkyTEM 504 system was used with a 488 m² transmitter coil with 4 turns and ~95 A current for HM measurements. This resulted in a HM moment of ~185,440 Am². In 2018, an improved SkyTEM 312 system with a transmitter coil of 341 m² with 12 turns and ~101 A current for HM measurements was employed. This resulted in a HM moment of ~450,120 Am². The specifications of the two system are listed in Table 1.

Compared to the ground-based TEM approach, the advantage of the airborne systems is of course the ability to collect datasets with large spatial coverage. TEM data are collected with the airborne approach as the aircraft flies at an average flight speed of 10 m/s. Data collected at short spatial intervals (e.g. 30–50 m flight distance) is averaged together as a single data recording and assigned to the location at the center of the averaging interval. Airborne data is commonly inverted to produce a suite of 1D-depth profiles (models) of the electrical conductivity as function of depth below the surface. 2D or 3D structures are mapped by constraining together nearby 1D models, where each 1D model thus corresponds to one data recording determined by the stacking

Table 1

Transmitter/receiver coil dimension, moment, and stacking time for low-moment (LM) and high-moment (HM) measurements. The repetition frequency for measurements is 30 Hz for HM SkyTEM and ~19 Hz for HM ground-based TEM system.

		SkyTEM 2011	SkyTEM 2018	Ground-based system
Transmitter coil area		488 m ²	341 m ²	10,000 m ²
Current	LM	~9.5 A	~6 A	~3.6 A
	HM	~95 A	~110A	~45 A
Number of turns in transmitter	LM	1 turn	2 turns	1 turn
	HM	4 turns	12 turns	1 turn
Moment	LM	4636 Am ²	4092 Am ²	36,000 Am ²
	HM	185,440 Am ²	450,120 Am ²	450,000 Am ²
Stacking time		1–4 s	1–4 s	600–900 s
Stack size	HM	30–120 transients	30–120 transients	11,000–17,000 transients

(averaging) of data from 30 to 50 flight meters. See section on inverse modelling.

3.2. Ground-based TEM

Ground-based TEM systems often use a large transmitter coil, typically in a square form with a side length of 40–100 m, deployed on the ground surface. The receiver coil, also deployed on the ground surface, is typically smaller in dimension and often located at the center of the transmitter coil (e.g. a central-loop configuration) as shown in Fig. 2a. The ground-based TEM system employed in this study has a 100 m × 100 m transmitter coil with a 10 m × 10 m receiver coil with two turns in a central-loop configuration. With a current amplitude of ~45 A for HM measurements, the transmit moment was ~450,000 Am² (Table 1). During the measurement, the ground-based systems remain in a fixed location and thus provide information about the subsurface in the immediate vicinity of the laid out loops.

The collection speed of ground-based TEM data varies depending on loop-size, terrain, and a number of other factors, but common production rates is between 5 and 20 soundings per day. For the ground-based data presented in this paper, an average of five soundings were collected during 6–7 h of field work with a team of 3–4 persons operating on difficult permafrost and ice surfaces. In practice, the team was flown out to the first location and then walked between the sounding with the 100 kg equipment on a sledge (Fig. 2b). In difficult terrain, the equipment had to be carried in backpacks. 10–15 min of data stacking was used at each location. With a repetition frequency of ~19 Hz for the HM measurements, this means that each sounding consists of 11,000–17,000 stacks, which are averaged together to one transient measurement (Fig. 4), which in the end produces one 1D-depth profile of the electrical conductivity beneath the center of the transmitter coil. Given the time

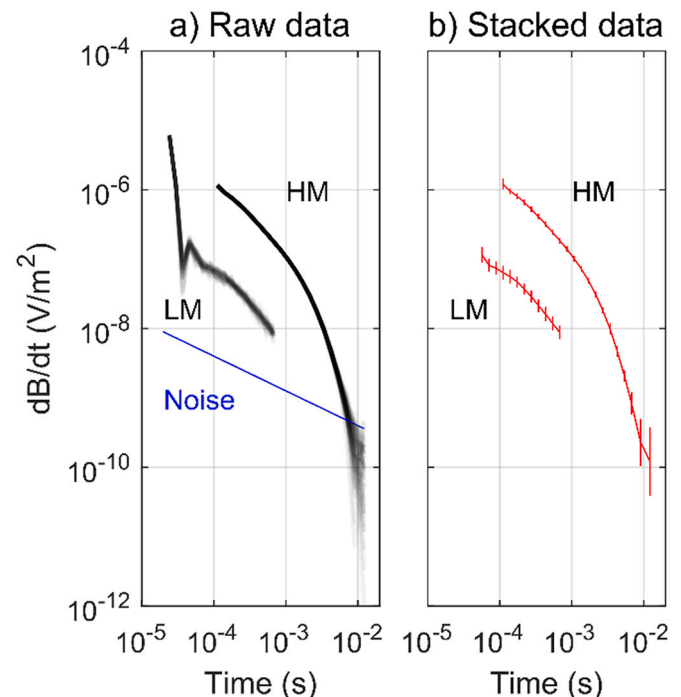


Fig. 4. Example of stacking of ground-based TEM data from the Canada Glacier. a) The raw data recordings for low-moment (LM) and high-moment (HM) measurements. Dark colour indicates high density of recordings. The noise level, which has the trend $t^{-1/2}$, is plotted in blue. b) The stacked data transient with two standard deviation error bars. Negative data were removed before the stacking, which explains the missing gates in the stacked LM data. (For interpretation of the references to colour in this figure legend, the reader is referred to the web version of this article.)

used for transportation and setting up the loops, a 10–15 min stacking time is easily justified. The effect of the stack size on the signal-to-noise ratio is discussed in the following.

3.3. Signal-to-noise ratio

As previously described, the DOI of a TEM sounding is influenced by several factors including the transmitter moment, the natural noise level, data stacking, and the conductivity of the subsurface. The airborne (2018 edition) and ground-based TEM systems employed in the McMurdo Dry Valleys have approximately the same transmitter moment for HM measurements (Table 1). However, a significant difference between the two TEM approaches lies in the duration of the measurement at any particular location. With the airborne approach, data is collected as the aircraft flies, which limits the data-averaging interval (stacking time) for each sounding to a few seconds. Longer averages are possible but given a fixed flight speed of approx. 100 km pr. hour this would reduce the lateral resolution and result in larger spacing between the resulting models. In contrast, the static ground-based system can collect data for much longer periods of time, providing much larger stack sizes for each sounding. The large stack sizes make it possible to diminish random background noise by averaging the repeated measurements, which significantly improves data quality. This is particularly important in the late times of the TEM signal, where the signal-to-noise ratio is the poorest. Fig. 3 shows an example of a ground-based and an airborne transient after stacking, where the late time-gates of the airborne data has been deleted due to noise.

The signal-to-noise ratio is, in general terms, proportional to the square root of the stack size (Spies, 1988). The DOI is roughly proportional to the signal-to-noise ratio raised to the 1/5 power (Spies, 1988), which means that in order to double the DOI, the signal-to-noise ratio should be increased by a factor 32. For the survey presented in this study, the number of stacks per sounding is ~ 120 for the airborne HM and $\sim 17,000$ for ground-based HM (Table 1). Consequently, the signal-to-noise ratio is approximately 12 times larger for the ground-based system given that the transmitter moments are about the same. This potentially means that the ground-based approach will get a factor 1.6 increase on the DOI relative to the airborne approach due to the effect of data stacking alone. However, these general terms only work as a rule of thumb, as they do not take all the factors affecting the DOI into account. Therefore, before presenting the resistivity profiles obtained from the measured airborne and ground-based data, we present the sensitivity of the two approaches and show how a layered subsurface with structures of different resistivity influences the DOI as well.

3.4. Inverse modelling

To convert the measured TEM data into 1D resistivity profiles (or models) an inversion of the data is performed. Here, a chosen misfit/cost/objective function is minimized to obtain a final model that best fits the recorded data. In this study, we have used the inversion software AarhusInv (Auken et al., 2015), which uses a deterministic gradient-based approach to invert the data.

For the ground-based data, the soundings are inverted separately, each producing a 1D-depth profile (model). The layer thickness is fixed in the inversion, so we only invert for the resistivity value of each layer. To stabilize the inversion process, the resistivity values of successive layers in a 1D model are constrained together producing a smoother transition from layer to layer. This smoothness is controlled by a vertical constraint parameter. For the airborne data, a suite of 1D models is produced due to the continuous data sampling. Apart from the same vertical constraints as used for ground-based data inversion, the 1D airborne models are also constrained horizontally to produce smooth continuous 2D resistivity profiles (see Auken and Christiansen, 2004). As less variation is expected in the horizontal direction, the smoothness constraints here are tighter compared to the vertical direction, as more

variation in resistivity is expected between the horizontal layering compared to within each layer.

For each 1D model, ground-based and airborne, the DOI is computed and added to the resulting resistivity profile to illustrate to what depth the resulting resistivity values can be considered reliable. The DOI is computed following Christiansen and Auken (2012), where the cumulative sensitivity (from the bottom up) of the final resistivity 1D models are calculated and the DOI is defined as the depth at which 90% of the sensitivity lies above. This approach to computing the DOI accounts for the resistivity model, the signal-to-noise ratio of the data (thus also the transmitter moment and the stacking), and the sensitivity pattern of the system.

4. Sensitivity for ground-based and airborne TEM

The resolution capability of a given TEM system can be visualized by its sensitivity, which is defined as the derivative of the measured data at a certain time (gate) with respect to the electric conductivity of the subsurface. The sensitivity thus describes how different parts of the subsurface contribute to the measured data. For a given point in the ground, a high sensitivity value means that a change in the conductivity (or resistivity) at this point will have a large impact on the measured data and vice versa.

Fig. 5 shows the sensitivity computed for the ground-based (Fig. 5a-c) and airborne TEM system (Fig. 5d-f) employed in this study. The sensitivity has been calculated following Christensen (2014) and is computed for the actual transmitter-receiver geometry and the transmitter current waveform of the two systems. The plots are shown for two time gates: 10^{-4} s (LM) and 10^{-3} s (HM). The sensitivity at each time gate is normalized by the maximum absolute sensitivity at the given time, making the plotted sensitivity a relative one between 0 and 1, illustrating the relative distribution of sensitivity in the ground. The 0.01, 0.1 and 0.5 contours of the sensitivity distributions are shown with the black lines. The figure shows that the sensitivity diffuses down and outward from the transmitter coil with time.

To illustrate how the sensitivity - and thus the DOI - changes with time during a TEM measurement, a footprint is often defined. Here, we define a footprint depth as the maximum depth of the 0.01 contour as a function of time after the start of the current turn-off in the transmitter coil. The footprint depth is plotted in Fig. 5g for LM and HM measurements using the airborne (blue) and ground-based (red) TEM systems. Fig. 5g shows that both the minimum and maximum footprint are deeper for the ground-based TEM system compared to the airborne. This means that the ground-based system can potentially resolve deeper structures, but that the airborne system has a better resolution closer to the surface. However, the computation of the sensitivity patterns only considers the geometry of the TEM systems and the resistivity of the ground, but not the different signal-to-noise ratios (due to data stacking and transmitter moment) that can be obtained with different systems.

To account for the difference in signal-to-noise level between the ground-based and airborne TEM approach applied in this study, which is mainly due to data stacking, the footprint curve in Fig. 5g is cut at $t = 3 \cdot 10^{-3}$ s for the airborne data and at $t = 5 \cdot 10^{-3}$ s for the ground-based data (Figs. 3 and 4), which are the approximate times after the current cut-off, where the field data signal drops below the noise level. Consequently, the maximum footprint is 460 m for the airborne approach and 725 m for the ground-based approach (Fig. 5g). However, these values should only be seen as relative ones, because the sensitivity also depends on the resistivity of the ground and by increasing the resistivity, the sensitivity will increase and spread further away from the system (down and outwards). For the comparative study in Fig. 5, we have used a homogenous ground with a resistivity of 100 Ωm , which approximates to the resistivity of Lake Vanda and is the center of the observed resistivity range (0.1–10,000 Ωm) in the log space, but increasing the resistivity would increase the footprint. For instance, for glacier ice and permafrost with a resistivity above 1000 Ωm , the footprint would

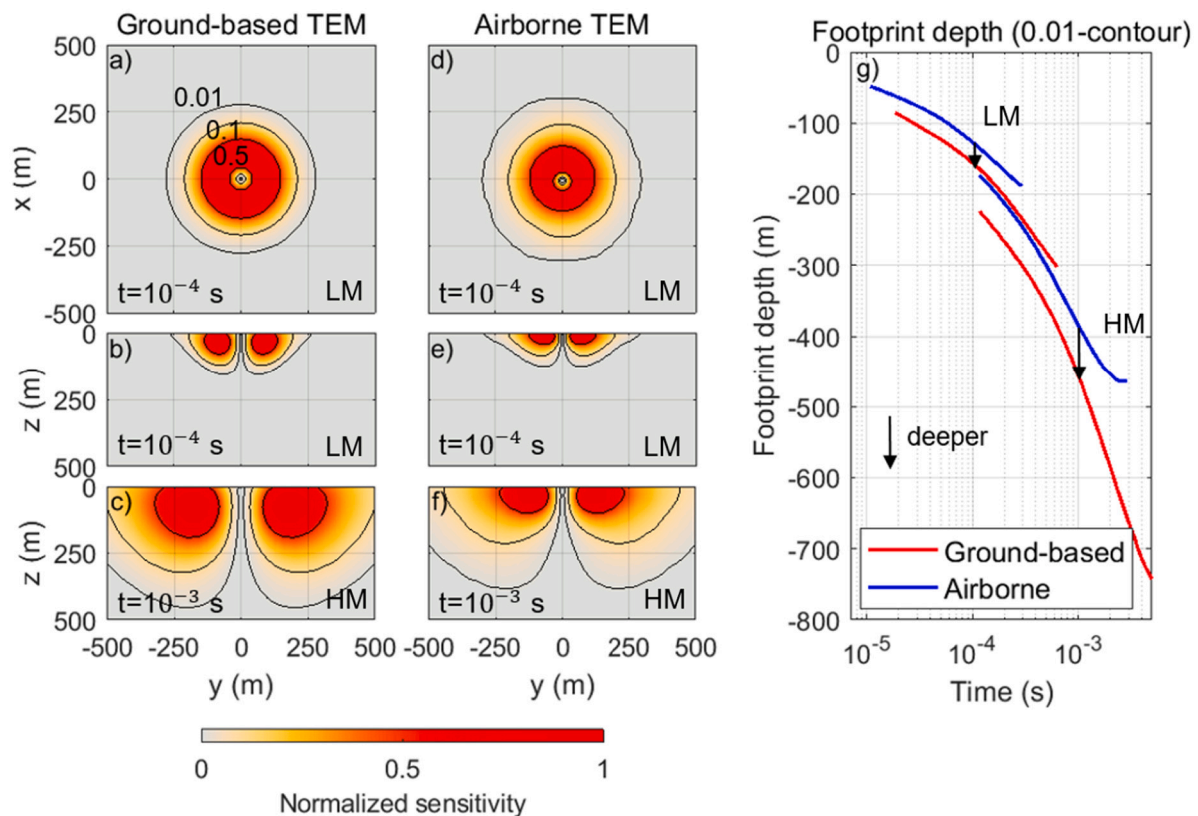


Fig. 5. Sensitivity distributions and footprints for the ground-based TEM (a-c) and airborne TEM system (d-f). The sensitivity is modelled for a homogenous subsurface of $100 \Omega\text{m}$ with the transmitter coil centered around $(x,y) = (0,0)$, and a flight direction along the x -axis and a flight height of 40 m for the airborne system. The sensitivity is normalized by the maximum sensitivity at the given time and is shown as the xy -planes ($z = 0$) and the yz -plane ($x = 0$) for low-moment (LM) time 10^{-4} s (a,b,d,e) and high-moment (HM) time 10^{-3} s (c,f). The black lines are the 0.01, 0.1, and 0.5 contours. The maximum depth of the 0.01-contour is plotted as a function of time in (g) defining a footprint depth, where the red curve is the footprint depth if the ground-based system (low and high moment) and the blue curves are the airborne system. (For interpretation of the references to colour in this figure legend, the reader is referred to the web version of this article.)

increase, but the relative difference between the ground-based and airborne system would still be the same as in Fig. 5.

Another complexity is added to the sensitivity patterns when layers with different resistivity are introduced. In general, the current induced in the ground has a larger density in conductive layers. Fig. 6 illustrates how this changes the sensitivity distributions in a polar environment with a glacier (resistive material, $3000 \Omega\text{m}$) on top of a brine layer (conductive material, $100 \Omega\text{m}$) on top of bedrock (resistive material, $1000 \Omega\text{m}$). Fig. 6 shows that the maxima of the sensitivity distributions quickly diffuse out and downwards to the conductive middle layer (Fig. 6b-c) and then stays in this conductive layer instead of diffusing into the resistive bedrock at the later times (Fig. 6d). The conductive layer thus acts as a shield (or wave guide) for the current over the resistive layer and the measured data will therefore contain limited information about the interior of the bedrock.

Combined, the sensitivity distributions and footprints show that the ground-based TEM system is potentially more sensitive to the deeper parts of the subsurface and thus can resolve deeper layers. Enhanced by the possibility of data stacking, this means that the ground-based approach will have a much larger DOI compared to the airborne approach in a homogenous environment. However, in an environment where conductive units are present (e.g. brine layers below glaciers), this will decrease the DOI of both approaches.

5. Comparison of ground-based and airborne resistivity sections

To investigate the consistency between the ground based and airborne data, three resistivity cross sections are illustrated in Figs. 7, 8, and 9. The resistivity cross-section are computed from the TEM data

using the geophysical inversion software AarhusInv where the airborne and ground-based data have been inverted individually.

5.1. Taylor Glacier

Consider first Fig. 7, which transects the Taylor Glacier along a line running parallel to the valley. Fig. 7 top-panel shows the location of the cross section superimposed on a satellite image of Taylor Glacier, the locations of airborne EM data collected in 2011 and 2018 are illustrated in orange and purple, respectively, while ground based EM sites are illustrated by red dots. The airborne data offers dense coverage of Taylor Glacier. Fig. 7 bottom-panel illustrates the resistivity cross section, where the y -axis corresponds to elevation above sea-level (effectively a depth axis) and the x -axis corresponds to the lateral position along the transect, with the left- and right-hand side of the image corresponding to the western and eastern most portions of the transect. Colors indicate the estimated electrical resistivity at each location in the subsurface, where purples correspond to very high resistivity values that are interpreted to be glacier ice as ice is expected to be very highly resistive. At the base of the glacier, a low resistive unit is observed.

Previous studies using electric resistivity tomography on glacier ice have measured resistivity values in the range of $10^4 - 10^8 \Omega\text{m}$ (e.g. Hochstein, 1967; Glen and Paren, 1975). Using the TEM method, the resistivity value of the glacier ice cannot be determined quantitatively, due to the previously described low sensitivity to highly resistive layer. However, the low resistivity unit at the base of the glacier is moderately to well-resolved with a resistivity of $20 \pm 8 \Omega\text{m}$. Given the low resistivity values and thickness of the overlying ice, this low resistivity layer is interpreted to be an unfrozen brine-saturated sediment at the base of the

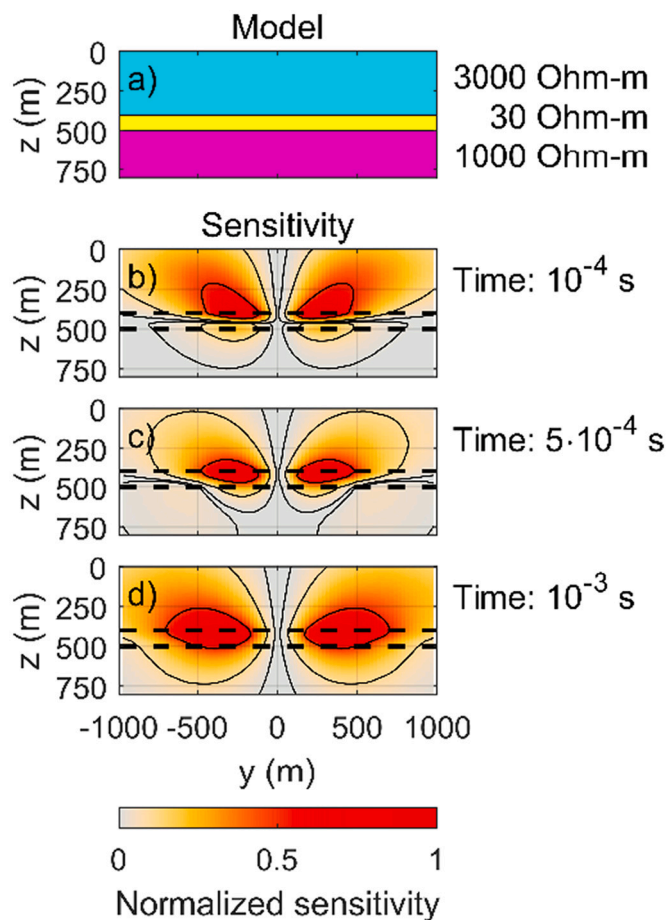


Fig. 6. Sensitivity distribution for ground-based TEM in a three-layer model with a conductive middle layer. This corresponds to a glacier overlaying a brine which in turn overlays bedrock. a) The resistivity model with three layers. b-c) The yz -plane ($x = 0$) of the normalized sensitivity distribution for three different time gates. The distributions are computed for the high moment (HM) ground-based TEM system and normalized by the maximum sensitivity at the given time. The dashed lines are the layer boundaries.

glacier (Mikucki et al., 2015). Brine has been observed to episodically discharge from the glacier (Badgeley et al., 2017) supporting this interpretation. The resistivity of the discharge has been measured to be below $0.17 \Omega\text{m}$ (Mikucki et al., 2009). In the east side of the profile, the glacier reaches Lake Bonney, which is approximately 40 m deep and has a permanent ice cover that fluctuates between 3 and 6 m in thickness (Spigel and Priscu, 1996; Obryk et al., 2014). Previous in situ measurements of the lake water show an increase in salinity with depth, which is correlated to a decrease in resistivity from $9 \Omega\text{m}$ in the top to $0.1 \Omega\text{m}$ at the bottom (Obryk et al., 2014; Mikucki et al., 2015). In the resistivity section in Fig. 7, the lake is seen as a very low resistive layer (blue colour, below $1 \Omega\text{m}$) with a more resistive upper layer (yellow-green colour, $\sim 25 \Omega\text{m}$), whose 8 m thickness corresponds reasonably well to the thickness of the permanent ice cover taking into account the discretization of the resistivity profiles.

Now we focus on the comparison of the airborne and ground-based resistivity results. In Fig. 7, the ground-based resistivity results (marked with black outlines) are plotted on top of the airborne results. The airborne and ground-based results are consistent with one another, as expected, estimating similar absolute resistivity values in the ice and underlying brines, as well as identifying consistent depths to the lower interface. Forming a profile from only the ground-based results would of course provide a coarser image, but the same conceptual model could be arrived at in this example.

For each 1D depth-profile – ground-based and airborne - the DOI is illustrated by the white shadow on top of the resistivity section, meaning that the resistivity value underneath this shadow is poorly or unresolved. The airborne resistivity profiles mainly contain data from the 2018 SkyTEM survey, but in locations where the 2011 data is used, the DOI is seen to move closer to the surface (e.g. $x = 6000$ m), due to the smaller transmitter moment of the 2011 SkyTEM system. The DOI for the ground-based and airborne data sets are similar at this site as it is mainly controlled by the resistivity contrasts in the subsurface and not by the signal-to-noise ratio.

5.2. Canada glacier

A transect over Canada Glacier is shown in Fig. 8. The top-panel illustrates the location of the transect, with the airborne and ground-based locations illustrated by the dots in the same colour scheme as in Fig. 7. The Canada Glacier separates two lakes, Lake Hoare and Lake Fryxell to the west and east, respectively. The transect runs down the length of the glacier (North to South), perpendicular to the valley axis. A similar structure is observed at Canada Glacier as in the previous example, where the resistivity profile again shows a thick resistive upper layer (the glacier ice) underlain by a lower resistivity layer. The ground-based (black outlined bars) and airborne data again agree well with one another, estimating similar resistivity values and depths to the lower interface. A transect of the full Taylor Valley, which also traverses Canada Glacier, formed from the 2011 airborne data, also shown here, is discussed in Mikucki et al. (2015). Here, the low resistivity layer at the base of Canada Glacier, which is interpreted as a layer of brine rich sediment, can be seen to extend underneath the neighboring lakes Hoare and Fryxell.

The resistivity profile of Canada Glacier contains both 2011 and 2018 SkyTEM data. The DOI plotted on top of the profile shows that the 2018 data have a better resolution at depth due to the higher transmitter moment (Table 1), seen for instance at $x = 2600$ – 2900 m. At the northern part of the profile (left side of the figure), the ground-based soundings have a deeper DOI compared to the airborne data, which is caused to the absence of high conductivities.

5.3. Lake Vanda

Fig. 9 illustrates a third example, where measurements were conducted over Lake Vanda, the largest lake in the McMurdo Dry Valleys. The locations of the transect, the airborne, and the ground-based data are illustrated in Fig. 9 top-panel (same colors as Figs. 7 and 8). Fig. 9 bottom-panel shows the resulting resistivity cross section. The maximum lake depth is 76 m and the water column is characterized by a steep salinity gradient with a measured water resistivity of $\sim 20 \Omega\text{m}$ at the surface and down to $\sim 0.1 \Omega\text{m}$ at the bottom (Castendyk et al., 2016). The bulk waters of Lake Vanda correspond to the teal region from ~ 3 to 8 km in the profile. The low resistivity layer (dark blue) sits at elevations just above and beneath the lake bottom suggesting the presence of saline lake water as well as sediments saturated with high salinity brines. The top of the low resistivity layer (transition from green to blue colors, from $20 \Omega\text{m}$ to $<5 \Omega\text{m}$) corresponds well with a jump in salinity measured at ~ 55 m depth (Castendyk et al., 2016). To the west (~ 1.5 to 2.5 km), a more complicated structure is observed with a low resistivity layer overlain by a high resistivity layer, which can be interpreted as 3D effects from the surrounding bedrock, which are visible here because the lake is very narrow and the sensitivity of the EM measurements extent beyond the lake shores. At ~ 1.5 km, another low resistivity layer is observed close to the surface, which corresponds to the lake's "tail" that can be seen in the left side of Fig. 9 top-panel. These structures highlight an advantage of the airborne system's ability to provide denser lateral resolution, where the sparse ground-based measurements do not convey the continuity of this local structure. Overall, there is again good agreement between the ground-based and airborne methods. The

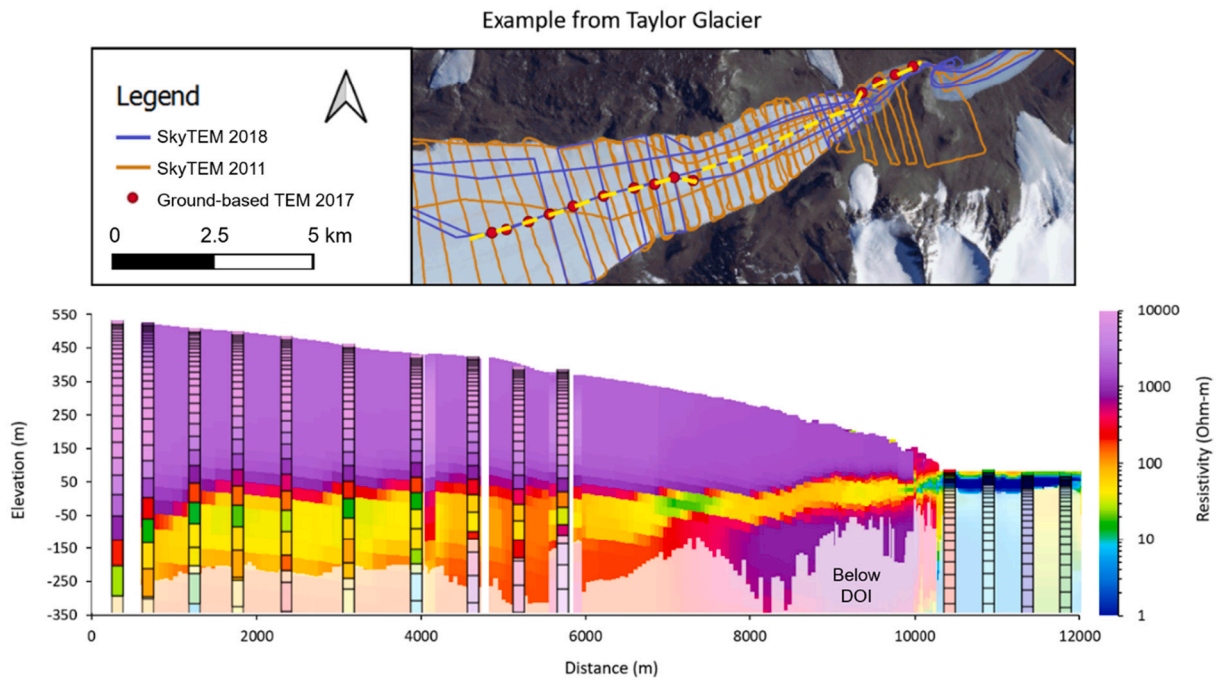


Fig. 7. Top: Map of the Taylor Glacier and the collected airborne TEM (purple and orange lines) and ground-based TEM (red dots) data. The yellow dashed line shows the location of the profile shown below. Bottom: The resistivity profile is plotted with the densely sampled airborne data as the background with the ground-based data on top, which is shown here with black boarders. The DOI is illustrated by the white shadow on top of the resistivity profile. (For interpretation of the references to colour in this figure legend, the reader is referred to the web version of this article.)

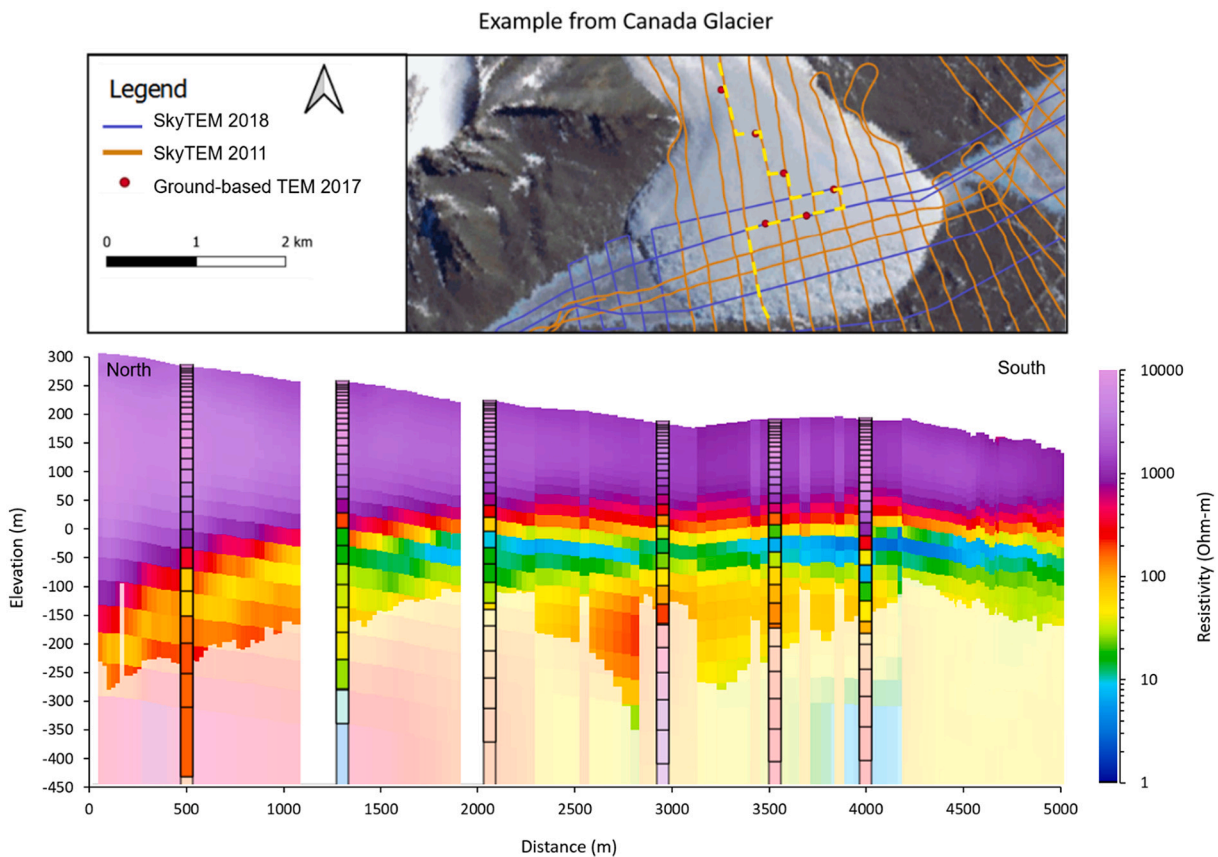


Fig. 8. Top: Map of the Canada Glacier and the collected airborne TEM (purple and orange lines) and ground-based TEM (red dots) data. The yellow dashed line shows the location of the profile shown below. Bottom: The resistivity profile is plotted with the densely sampled airborne data as the background with the ground-based data on top, which is shown here with black boarders. The DOI is illustrated by the white shadow on top of the resistivity profile. (For interpretation of the references to colour in this figure legend, the reader is referred to the web version of this article.)

Example from Lake Vanda

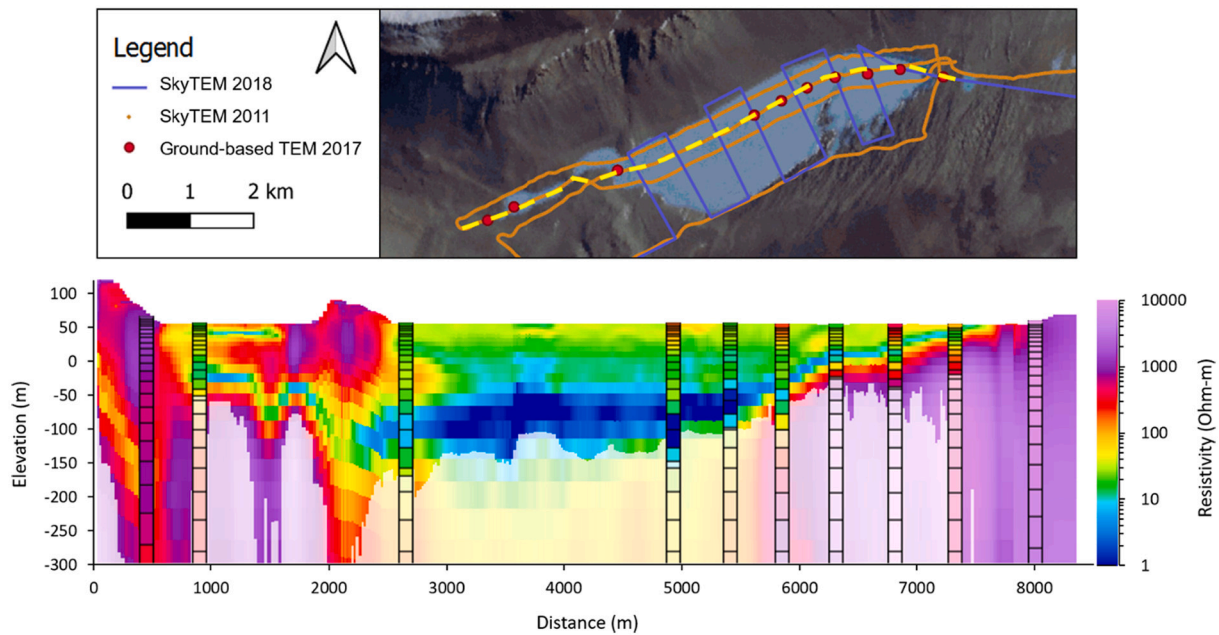


Fig. 9. Top: Map of the Lake Vanda and the collected airborne TEM (purple and orange lines) and ground-based TEM (red dots) data. The yellow dashed line shows the location of the profile shown below. Bottom: The resistivity profile is plotted with the densely sampled airborne data as the background with the ground-based data on top, which is shown here with black borders. The DOI is illustrated by the white shadow on top of the resistivity profile. (For interpretation of the references to colour in this figure legend, the reader is referred to the web version of this article.)

boundaries and the resistivity of the lake are well-resolved while the high resistivity values of the bedrock ($x = 6000\text{--}8000$ m in Fig. 9) is only moderate to poorly determined.

6. Discussion

6.1. TEM in polar environments

Transient electromagnetics is well suited to polar environments, where many common targets correspond to strong contrasts in electrical resistivity. It is also common for the near-surface material to be highly resistive, as in the case for the very resistive glacier ice, frozen ground, or when bedrock is close to surface. In these cases, the DOI can be increased because a resistive overburden only weakly attenuates the TEM signal. However, if the resistive overburden is very thick it can be difficult to produce a TEM signal that exceeds the input noise levels of the system. In this scenario, one is still able to infer that the background is highly resistive and likely absent of units with lower resistivity (at least down to the DOI for the system). This can still provide usable information, but one is unable to quantitatively comment on the resistivity of the subsurface. This scenario was encountered in many locations throughout the McMurdo Dry Valleys – for instance on the Taylor Glacier. When the ice overburden becomes too thick relative to the resolution capabilities of the TEM system (exceeding 600–700 m in thickness), only noise is measured (and no earth response) and a resistivity depth profile representative of the subsurface cannot be produced. In general, the absolute resistivity values of the glacier ice were poorly resolved while the thickness of the glacier ice, resistivity of brine layers below the glaciers, the glacier lakes, and the bedrock were moderate to well-resolved using both TEM methods.

6.2. Ground-based and airborne TEM data

Ground-based and airborne configurations produce consistent estimates of electrical resistivity in the subsurface. The primary differences

come in imaging resolution – with airborne offering far improved lateral resolution. In certain cases, like in the glacier examples, reduced lateral resolution is not a significant detriment to the interpretation. The main structures and their lateral extent can still be resolved. However, in cases with more lateral heterogeneity, as in the Lake Vanda example, the coarser ground-based resolution may lead to challenges resolving small-scale structures. In terms of vertical resolution, both airborne and ground-based systems provide similar performance. In a scenario with a homogenous ground, the ground-based system has a larger penetration depth and DOI due to its larger dimensions and longer stacking time. However, if a conductive brine layer is located below the glacier ice, the sensitivity drops quickly below this layer, hence, the two systems have similar DOI. The system specifications can be tailored to improve performance of the depth interval of interest. For example, if shallow depths are of chief interest, smaller moment systems can be employed to enhance shallow resolution. Alternatively, if deep penetration is required larger moment systems can enhance depth penetration at the expense of decreased shallow resolution.

One of the primary advantages of the ground-based methods is that they are more accessible to a wider range of studies. That is, the systems are much cheaper to deploy and can be operated after minimal training by small teams. They can also be readily transported over large distances by ATV or snowmobile. In contrast, the airborne methods have high mobilization costs because of the need to transport the TEM equipment in a shipping container to the study region and to involve an aircraft capable of carrying the system. Moreover, an airborne TEM survey necessitates the use of specially trained personnel. Hence, airborne TEM is generally better suited to projects interested in significant spatial coverage and with larger budgets and logistical support. Data handling is also simpler for ground-based measurements, as they result in much smaller data sets that can be readily processed and interpreted in a number of different software packages. Airborne datasets are typically much larger and complex and therefore require a higher level of training and familiarity with TEM data. However, the two approaches are extremely complimentary. Ground-based campaigns can serve as

valuable preliminary surveys or as follow-up ground-truth measurements that can focus on features first detected in airborne data. For example, the 2017 ground-based measurements discussed in this work were key in planning follow-up airborne surveys in 2018 and confirmed that high quality TEM data could be collected in a number of new places throughout the dry valleys.

7. Conclusions

Transient electromagnetic methods are well-suited to image subsurface structures in polar settings when conductive targets are present. Ground-based TEM and airborne TEM approaches are shown to produce consistent results in several examples in the McMurdo Dry Valleys. Although airborne TEM provides high-resolution imaging with unparalleled spatial coverage, ground-based TEM measurements remain a valuable tool. The ground-based approach is much more accessible than airborne, and is well suited to standalone mapping campaigns as well as preliminary scouting or follow-up investigations to airborne studies.

CRediT authorship contribution statement

Line M. Madsen: Methodology, Formal analysis, Visualization, Writing – original draft, Writing – review & editing. **Thue Bording:** Methodology, Formal analysis, Visualization, Writing – original draft, Writing – review & editing. **Denys Grombacher:** Methodology, Formal analysis, Visualization, Writing – original draft, Writing – review & editing. **Nikolaj Foged:** Methodology, Formal analysis, Visualization, Writing – review & editing. **Neil Foley:** Methodology, Formal analysis, Writing – review & editing. **Hilary A. Dugan:** Methodology, Formal analysis, Writing – review & editing. **Peter T. Doran:** Methodology, Formal analysis, Writing – review & editing. **Jill Mikucki:** Methodology, Formal analysis, Writing – review & editing. **Slawek Tulaczyk:** Methodology, Formal analysis, Writing – review & editing, Supervision. **Esben Auken:** Methodology, Formal analysis, Writing – review & editing, Supervision.

Declaration of Competing Interest

None.

Acknowledgements

This work was supported by funding from VILLUM FUNDEN Grant No. 37172 to L.M. Madsen, NSF Grant No. 1644187 to S. Tulaczyk, and NSF Grant No. 1643687 to J. Mikucki. We are thankful for the logistical field support from the United States Antarctic Program, which enabled collection of our data. In particular, we thank the helicopter crews from PHI Inc., McMurdo helicopter coordinator Lindsay Steinbauer and her team, operators of the Marble Point helicopter refueling station, and our field support leader, Robin Carroccia.

References

Arcone, S.A., Kreutz, K., 2009. GPR reflection profiles of clark and commonwealth glaciers, dry valleys, Antarctica. *Ann. Glaciol.* 50, 121–129.

Auken, E., Christiansen, A.V., 2004. Layered and laterally constrained 2D inversion of resistivity data. *Geophysics* 69 (3), 752–761.

Auken, E., Christiansen, A.V., Fiandaca, G., Schamper, C., Behroozmand, A.A., Binley, A., Nielsen, E., Effersø, F., Christensen, N.B., Sørensen, K.I., Foged, N., Vignoli, G., 2015. An overview of a highly versatile forward and stable inverse algorithm for airborne, ground-based and borehole electromagnetic and electric data. *Explor. Geophys.* 2015, 223–235.

Auken, E., Boesen, T., Christiansen, A.V., 2017. A review of airborne electromagnetic methods with focus on geotechnical and hydrological applications from 2007 to 2017. In: *Book: Advances in Geophysics* edn. Elsevier.

Badgeley, J.A., Pettit, E.C., Carr, C.G., Tulaczyk, S., Mikucki, J.A., Lyons, W.B., 2017. An englacial hydrologic system of brine within a cold glacier: Blood Falls, McMurdo Dry Valleys, Antarctica. *J. Glaciol.* 63, 387–400.

Campbell, S., Affleck, R.T., Sinclair, S., 2018. Ground-penetrating radar studies of permafrost, periglacial, and near-surface geology at McMurdo Station, Antarctica. *Cold Reg. Sci. Technol.* 148, 38–49.

Castendyk, D.N., Obryk, M.K., Leidman, S.Z., Gooseff, M., Hawes, I., 2016. Lake Vanda: a sentinel for climate change in the McMurdo Sound Region of Antarctica. *Glob. Planet. Chang.* 144, 213–227.

Christensen, N.B., 2014. Sensitivity functions of transient electromagnetic methods. *Geophysics* 79, E167–E182.

Christiansen, A.V., Auken, E., 2012. A global measure for depth of investigation. *Geophysics* 77, WB171–WB177.

Clarke, G.K.C., 2005. 2005: SUBGLACIAL PROCESSES. *Annu. Rev. Earth Planet. Sci.* 33 (1), 247–276. <https://doi.org/10.1146/annurev.earth.33.092203.122621>.

Doran, P.T., McKay, C.P., Clow, G.D., Dana, G.L., Fountain, A.G., Nylen, T., Lyons, W.B., 2002. Valley floor climate observations from the McMurdo Dry Valleys, Antarctica, 1986–2000. *J. Geophys. Res.-Atmos.* 107. ACL 13-11-ACL 13-12.

Dugan, H., Doran, P., Tulaczyk, S., Mikucki, J., Arcone, S.A., Auken, E., Schamper, C., Virginia, R., 2015. Subsurface imaging reveals a confined aquifer beneath an ice-sealed Antarctic lake. *Geophys. Res. Lett.* 42, 96–103.

Foley, N., Tulaczyk, S., Auken, E., Schamper, C., Dugan, H., Mikucki, J., Virginia, R., Doran, P., 2016. Helicopter-borne transient electromagnetics in high-latitude environments: an application in the McMurdo Dry Valleys, Antarctica. *AEM resistivity in the Dry Valleys. Geophysics* 81, WA87–WA99.

Foley, N., Tulaczyk, S.M., Grombacher, D., Doran, P.T., Mikucki, J., Myers, K.F., Foged, N., Dugan, H., Auken, E., Virginia, R., 2019. Evidence for pathways of concentrated submarine groundwater discharge in East Antarctica from Helicopter-Borne electrical resistivity measurements. *Hydrology* 6, 54.

Foley, N., Tulaczyk, S., Auken, E., Grombacher, D., Mikucki, J., Foged, N., Myers, K., Dugan, H., Doran, P.T., Virginia, R.A., 2020. Mapping geothermal heat flux using permafrost thickness constrained by airborne electromagnetic surveys on the western coast of Ross Island, Antarctica. *Explor. Geophys.* 51, 84–93.

Glen, J.W., Paren, J.G., 1975. The electrical properties of snow and ice. *J. Glaciol.* 15 (73), 15–38.

Haas, C., Gerland, S., Eicken, H., Miller, H., 1997. Comparison of sea-ice thickness measurements under summer and winter conditions in the Arctic using a small electromagnetic induction device. *Geophysics* 62 (3), 749–757.

Hochstein, M., 1967. Electrical resistivity measurements on ice sheets. *J. Glaciol.* 6 (47), 623–633.

Kass, M.A., Maurya, P., Ingeman-Nielsen, T., Pedersen, J., Tomaskovicova, S., Christiansen, A.V., 2021. Towed transient electromagnetic survey results at Ilulissat, Greenland for water vulnerability and infrastructure planning. In: *NSG2021 2nd Conference on Geophysics for Infrastructure Planning, Monitoring and BIM*, Vol. 2021, No. 1. European Association of Geoscientists & Engineers, pp. 1–5.

Kavanaugh, J., Cuffey, K., 2009. Dynamics and mass balance of Taylor Glacier, Antarctica: 2. Force balance and longitudinal coupling. *J. Geophys. Res. Earth Surf.* 114.

Kozhevnikov, N.O., Antonov, E.Y., Zakharkin, A.K., Korsakov, M.A., 2014. TEM surveys for search of taliks in areas of strong fast-decaying IP effects. *Russ. Geol. Geophys.* 55 (12), 1452–1460.

Levy, J., 2013. How big are the McMurdo Dry Valleys? Estimating ice-free area using Landsat image data. *Antarct. Sci.* 25, 119.

Marchant, D.R., Head III, J.W., 2007. Antarctic dry valleys: Microclimate zonation, variable geomorphic processes, and implications for assessing climate change on Mars. *Icarus* 192, 187–222.

Mikucki, J.A., Pearson, A., Johnston, D.T., Turchyn, A.V., Farquhar, J., Schrag, D.P., Anbar, A.D., Prisco, J.C., Lee, P.A., 2009. A contemporary microbially maintained subglacial ferrous "ocean". *Science* 324 (5925), 397–400.

Mikucki, J.A., Auken, E., Tulaczyk, S., Virginia, R.A., Schamper, C., Sorensen, K.I., Doran, P.T., Dugan, H., Foley, N., 2015. Deep groundwater and potential subsurface habitats beneath an Antarctic dry valley. *Nat. Commun.* 6.

Minsley, B.J., Abraham, J.D., Smith, B.D., Cannia, J.C., Voss, C.I., Jorgenson, M.T., Walvoord, M.A., Wylie, B.K., Anderson, L., Ball, L.B., Szcz-Pan, M., Wellman, T.P., Ager, T.A., 2012. Airborne electromagnetic imaging of discontinuous permafrost. *Geophys. Res. Lett.* 39, L02503.

Navarro, F., Eisen, O., 2009. *Ground-Penetrating Radar in Glaciological Applications (In book: Remote Sensing of Glaciers)*. CRC Press, London.

Obryk, M.K., Doran, P.T., Prisco, J.C., 2014. The permanent ice cover of Lake Bonney, Antarctica: the influence of thickness and sediment distribution on photosynthetically available radiation and chlorophyll-a distribution in the underlying water column. *J. Geophys. Res. Biogeosci.* 119, 1879–1891. <https://doi.org/10.1002/2014JG002672>.

Pfaffling, A., Haas, C., Reid, J.E., 2007. Direct helicopter EM—Sea-ice thickness inversion assessed with synthetic and field data. *Geophysics* 72 (4), F127–F137.

Shean, D.E., Marchant, D.R., 2010. Seismic and GPR surveys of Mullins Glacier, McMurdo Dry Valleys, Antarctica: ice thickness, internal structure and implications for surface ridge formation. *J. Glaciol.* 56, 48–64.

Smith, A.M., Jordan, T.A., Ferraccioli, F., Bingham, R.G., 2013. Influence of subglacial conditions on ice stream dynamics: Seismic and potential field data from Pine Island Glacier, West Antarctica. *J. Geophys. Res. Solid Earth* 118, 1471–1482. <https://doi.org/10.1029/2012JB009582>.

Sørensen, K.I., Auken, E., 2004. SkyTEM—a new high-resolution helicopter transient electromagnetic system. *Explor. Geophys.* 35, 194–202.

Spies, B.R., 1988. Local noise prediction filtering for central induction transient electromagnetic sounding. *Geophysics* 53, 1068–1079.

- Spies, B.R., 1989. Depth of investigation in electromagnetic sounding methods. *Geophysics* 54, 872–888.
- Spigel, R.H., Prisco, J.C., 1996. Evolution of temperature and salt structure of Lake Bonney, a chemically stratified Antarctic lake. *Hydrobiologia* 321, 177–190.

- Wetherly, K.E., Irvine, R.J., Morrison, E., 2004. The Geotech VTEM time domain helicopter EM system. *ASEG Extend. Abstr.* 1–4.